



## Numerical parametric investigation of infiltration in one-dimensional sand–geotextile columns

Greg Siemens\*, Richard J. Bathurst

GeoEngineering Centre at Queen's – RMC, Civil Engineering Department, 13 General Crerar, Sawyer Building, Royal Military College of Canada, Kingston, Ontario, Canada K7K 7B4

### ARTICLE INFO

#### Article history:

Received 7 July 2009

Received in revised form

3 December 2009

Accepted 3 December 2009

Available online 18 February 2010

#### Keywords:

Infiltration

1-D column modelling

Sand

Geotextile

Unsaturated–saturated flow

### ABSTRACT

Geotextiles are routinely used in separation and filtration applications. Design of these systems is currently based on saturated properties of the geotextiles and the surrounding soils. However, in the field, soil and geotextile can be in an unsaturated state for much of their design life during which they are essentially hydraulically non-conductive. Periodic wetting and drying cycles can result in rapid and large changes in hydraulic performance of soil–geotextile systems. The writers have reported the results from physical water infiltration tests on sand columns with and without a geotextile inclusion. The geotextile inclusions were installed in new and modified states to simulate the influence of clogging due to fines and to broaden the range of hydraulic properties of the geotextiles in the physical tests. This paper reports the results of numerical simulations that were undertaken to reproduce the physical tests and strategies adopted to adjust soil and geotextile properties from independent laboratory tests to improve the agreement between numerical and physical test results. For example the paper shows that the hydraulic conductivity function of the geotextile must be reduced by up to two orders of magnitude to give acceptable agreement. The lower hydraulic conductivity is believed to be due to soil intrusion that is not captured in conventional laboratory permeability tests. The calibrated numerical model is used to investigate the influence of geotextile and soil hydraulic conductivity and thickness as well as height of ponded water at the surface on wetting front advance below the geotextile and potential ponding of water above the geotextile due to a capillary break mechanism. A simple analytical model is also developed that predicts the maximum ponding height of water above the geotextile based on two-layer saturated media and 1-D steady state flow assumptions. The analytical model is used to generate a design chart to select geotextiles to minimize potential ponding of water above the geotextile. Ponding can lead to lateral flow of water along the geotextile in reinforced wall, slope, embankment and road base applications.

© 2009 Elsevier Ltd. All rights reserved.

### 1. Introduction

Research and design of geotextiles for hydraulic applications such as filtration and separation have typically focused on saturated conditions. For example, design of geotextile filters uses the saturated hydraulic conductivity as well as the apparent opening size (AOS) or Filtration Opening Size (FOS) of the geotextile (Holtz et al., 1997; Koerner, 2005; Canadian Foundation Engineering Manual, 2006). However, a geotextile may be unsaturated for much of its lifetime since it de-saturates at very low suctions (typically equivalent to negative 1–2 cm of water). The hydraulic conductivity

of geotextiles can change by orders of magnitude as the geotextile moisture content changes between residual and saturated conditions. The large changes in hydraulic conductivity of the geotextile during wetting and drying cycles may be expected to have important consequences to hydraulic performance. It is for this reason that the unsaturated–saturated hydraulic properties of geotextiles have been the subject of investigation by a number of researchers. A review of related earlier work can be found in the paper by Bathurst et al. (2009). Of particular relevance to the current study are contributions by Bouazza et al. (2006), Cartaud et al. (2005), Knight and Kotha (2001), Krisdani et al. (2006, 2008), Lafleur et al. (2000), Nahlawi et al. (2007) and Stormont et al. (1997) on the isolation unsaturated–saturated properties of geotextiles. Important related contributions describing the unsaturated–saturated response of soil–geotextile columns have been reported by Bathurst et al. (2007, 2009), Ho (2000), Krisdani et al. (2008) and Stormont and Morris (2000). An excellent summary of experimentally

\* Corresponding author. GeoEngineering Centre at Queen's – RMC, Civil Engineering Department, 13 General Crerar, Sawyer Building, Room 2305, Royal Military College of Canada, Kingston, Ontario, Canada K7K 7B4. Tel.: +1 613 541 6000x6396; fax: +1 613 541 6218.

E-mail address: [Greg.Siemens@rmc.ca](mailto:Greg.Siemens@rmc.ca) (G. Siemens).

determined water characteristic curve data and relative hydraulic conductivity curve data available at the time for nonwoven geotextiles is provided by Iryo and Rowe (2003). Examples of fitting curves using van Genuchten (1980) equations are also provided. Iryo and Rowe (2005a, b) and Garcia et al. (2007) have reported the results of numerical modelling of geotextile reinforced slopes and embankments subjected to surface water infiltration loading.

The main objective of the work described in the current paper was to carry out a numerical parametric analysis of the influence of geotextile hydraulic properties on the 1-D response of initially unsaturated sand–geotextile columns subjected to surface water infiltration. The numerical simulations are used to expand the database of experimental 1-D column test results reported by Ho (2000) and Bathurst et al. (2007, 2009). The first step in the numerical investigation was to verify that the numerical model could satisfactorily reproduce the hydraulic response of the physical tests. It is shown that to do this the hydraulic conductivity of the geotextiles deduced from conventional permittivity tests must be reduced by up to two orders of magnitude to account for the influence of soil particle intrusion. Some of the same physical tests have been used by Iryo and Rowe (2003, 2004) to calibrate a 1-D numerical model for infiltration loading. However, there are important differences between the current study and this earlier work that are explained later in the paper. The calibrated model in the current study is then used to investigate the influence of geotextile hydraulic conductivity, thickness and permittivity, soil hydraulic conductivity and thickness, and surface boundary condition on 1-D sand–geotextile systems subjected to surface water infiltration. An analytical model is derived to predict ponding above the geotextile by assuming steady state flow conditions. The numerical results lead to recommendations for selection of geotextiles to minimize potential ponding of water above the geotextile that could cause lateral flow of water along the geotextile in reinforced wall, slope, embankment and road base applications.

## 2. Physical tests

A brief review of the 1-D column test methodology and materials is presented for completeness. The test apparatus is illustrated in Fig. 1. The Plexiglas column was about 2 m in height with an inside diameter of 10 cm. A control test was carried out with sand only and four other tests were carried out with a different geotextile layer located at about mid-height. The columns were prepared by pluviating sand into the water column and then draining the column to residual water content of the sand. Next a constant head of water (10 cm) was applied to the top of the column until a hydrostatic pore-pressure distribution was measured in the tensiometers. Tensiometers and conductivity probes were located along the column to record pore-water pressures (including suctions) and the location of the wetting front as the experiment progressed. Details of the physical tests, instrumentation, measurement interpretation, and the properties of sand and geotextile materials can be found in the papers by Bathurst et al. (2007, 2009).

### 2.1. Sand

The sand used in the physical tests is poorly graded sand (SP) according to the United Soil Classification System. The as-placed porosity of the pluviated sand was 0.52 and the saturated hydraulic conductivity of the sand was reported to be  $2.0 \times 10^{-3}$  m/s. The water retention characteristics of the sand were measured using a Tempe cell. The drying and wetting data points are plotted in Fig. 2 along with the fitted Fredlund and Xing (1994) curve for the wetting soil–water characteristic curve (SWCC) expressed as

$$\theta(\Psi, a, n, m) = C(\Psi) \frac{\theta_s}{\left\{ \ln \left[ e + \left( \frac{\Psi}{a} \right)^n \right] \right\}^m} \quad (1a)$$

$$C(\Psi) = 1 - \frac{\ln \left( 1 + \frac{\Psi}{\Psi_r} \right)}{\ln \left[ 1 + \left( \frac{1000000}{\Psi_r} \right) \right]} \quad (1b)$$

where  $\theta$  = water content,  $\Psi$  = suction;  $C(\Psi)$  = correction function,  $\theta_s$  = saturated water content, and  $a, n, m, \Psi_r$  = fitting parameters. The data obtained from the Tempe cell show the air entry value to be 0.5 kPa, with a water entry value of 2–3 kPa and a residual water content of 8% (gravimetric). Little hysteresis was observed as the wetting and drying data points are very close.

The column preparation procedure also provided an independent measurement of the SWCC. Following pluviating of the sand particles in water, the bottom valve was opened and water drained from the column until the sand came into equilibration with the free water boundary (Fig. 1). Equilibrium was determined when water stopped flowing from the column and the tensiometer measurements became constant. Next, very small samples of sand were extracted through the sampling ports along the height of the column and these samples used for gravimetric water content (GWC) analysis. Consistent measurements of approximately 9–10% GWC were measured for the five infiltration tests. These are plotted with open circles in Fig. 2 assuming a hydrostatic pore-pressure profile above the free water boundary. These in-situ column measurements taken prior to infiltration loading are considered to be more accurate than values using the Tempe cell. The initial gravimetric water content measurements correspond to about 1.1 kPa suction using tensiometer measurements from the five infiltration tests. In this investigation the SWCC was judged to be best fitted to the column measurements at low moisture content and using the Tempe cell values at saturated states (samples were not taken from the flooded column). The Fredlund and Xing (1994) curve is plotted in Fig. 2 over the practical wetting range of interest (<2 kPa suction) using the fitting parameters in Table 3.

### 2.2. Geotextiles

Two typical commercially available geotextile materials were used in the column tests and their relevant properties are given in Table 2. One material was a woven geotextile manufactured from polypropylene slit film monofilament. The second geotextile was a nonwoven manufactured from continuous entangled polypropylene filament. To simulate potential clogging which can reduce hydraulic conductivity (Palmeira and Gardoni, 2000) the geotextiles were modified by the addition of a kaolin powder. Infiltration tests were carried out on sand columns with new and modified geotextile inclusions to assess the impact of clogging on infiltration behaviour and to broaden the range of hydraulic properties for the geotextile inclusions.

For numerical simulations, the geotextile properties of interest are the thickness, saturated hydraulic conductivity and geotextile–water characteristic curve (GWCC). Geotextiles will compress under vertical pressure. In the column tests, geotextile inclusions were placed at 120 cm below surface. From one-dimensional compression tests performed on the geotextile specimens, this depth corresponds to a thickness ( $t_g$ ) of 1.8 mm and 3.8 mm for the woven and nonwoven geotextiles, respectively. In practice, geotextile thickness cannot normally be measured to an accuracy of  $\pm 0.1$  mm. According to ASTM D5199 (2004) the measurement repeatability limit is  $\pm 14\%$  for thickness of a geotextile under a 2 kPa load. This level of accuracy corresponds to  $\pm 0.25$  mm and  $\pm 0.53$  mm for the woven and nonwoven geotextiles, respectively. However,

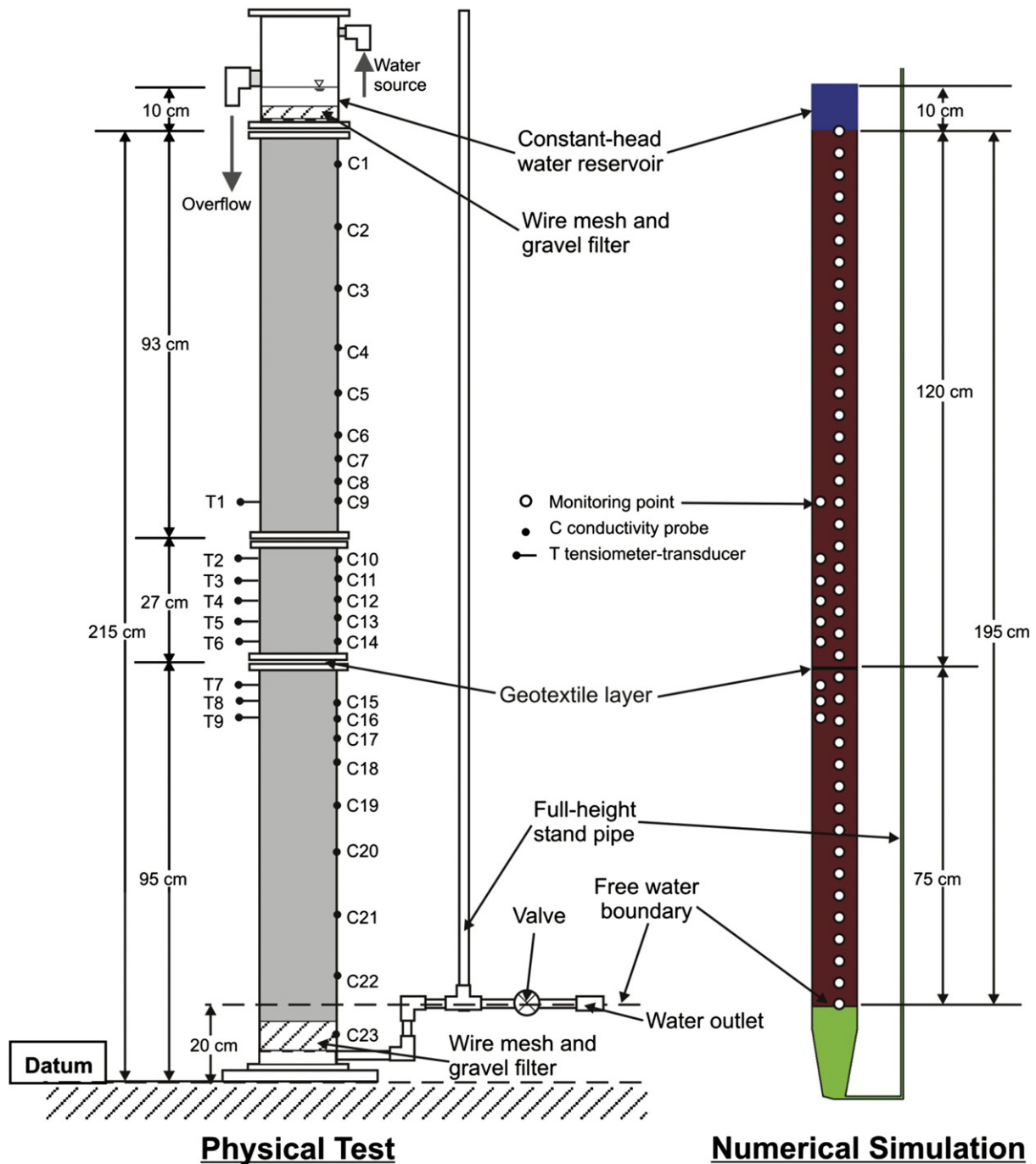


Fig. 1. Schematic of physical test column and numerical model.

numerical simulation results were found to be very sensitive to small changes in geotextile thickness. Therefore, geotextile dimensions were defined to this level of accuracy.

The permittivity ( $\Psi_g$ ) of the woven and nonwoven geotextile materials was measured in both the new and modified conditions (Bathurst et al., 2009). The measured values were converted to hydraulic conductivity using the equation

$$K_{\text{sat(geotextile)}} = \Psi_g \times t_g \quad (2)$$

where  $K_{\text{sat(geotextile)}}$  = saturated hydraulic conductivity in the direction normal to the plane of the geotextile (i.e. cross-plane

direction). [Palmeira and Gardoni \(2002\)](#) have demonstrated that the permittivity of a geotextile will vary with thickness. Hence, saturated hydraulic permeability should be determined using specimens under confining pressure as described in [ASTM 5493 \(2003\)](#). This was not done in the original experimental program as explained by [Bathurst et al. \(2009\)](#). However, the saturated permeability determined from an unconfined test using ([ASTM D4491, 2004](#)) and Equation (2) was corrected using the permittivity from the unconfined test multiplied by the estimated compressed thickness of the geotextile under 1 m of soil.

The GWCCs for the woven and nonwoven geotextiles in new and modified states were measured using a suction plate apparatus. The

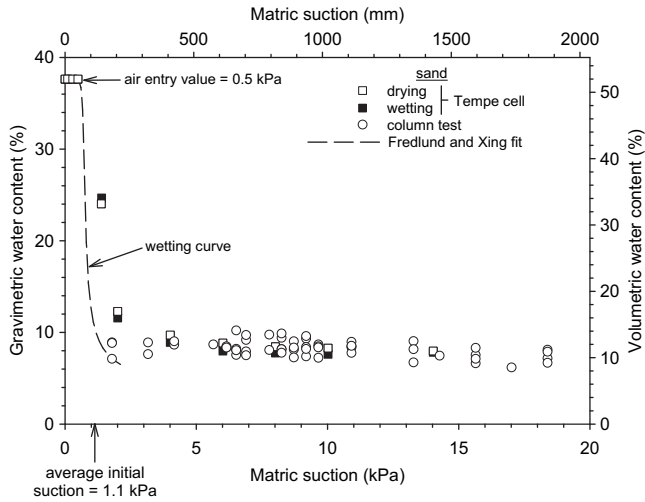


Fig. 2. Soil–water characteristic curve for sand.

points measured during both drying and wetting are shown in Fig. 3 along with Fredlund and Xing (1994) fits for the wetting curve. Fitted parameters for the wetting curves can be found in Table 3. The plots show that the transition suction range (suction range between the air entry value and residual saturation) is relatively small. Similar steep GWCC curves have been reported by Bouazza et al. (2006), Cartaud et al. (2005), Lafleur et al. (2000), Knight and Kotha (2001), Krisdani et al. (2006, 2008), Nahlawi et al. (2007) and Stormont et al. (1997). The lower transition on the wetting curves is in the vicinity of 0.05 kPa for the new-nonwoven geotextile up to about 0.6 kPa for the modified-woven geotextile. The steepness of the GWCC data poses a challenge when attempting to fit curves to the data points. However, in the simulations that follow it was found that beyond a critical slope value there was no influence on column test results. Hence, a close fit to the measured data points in the transition zone was difficult to achieve but not necessary to achieve a good match between physical and numerical results. Similarly, at high suction values corresponding to residual moisture content, it was not necessary to accurately model the GWCC tails to achieve good quantitative predictions.

The corresponding sand and geotextile unsaturated hydraulic conductivity curves are plotted in Fig. 4. The Leong and Rahardjo (1997) fitting curve was used to model the unsaturated portion of the hydraulic conductivity curves. This equation is expressed as

$$K(\Psi) = K_{sat} \left[ \frac{1}{\left\{ \ln \left[ e + \left( \frac{\Psi}{a} \right)^n \right] \right\}} \right]^p \quad (3)$$

where  $K(\Psi)$  = unsaturated hydraulic conductivity;  $K_{sat}$  = saturated hydraulic conductivity and,  $p$  = fitting parameter. Comparing the geotextile and sand unsaturated hydraulic conductivity curves (Fig. 4) shows that the geotextile hydraulic conductivity is lower than the sand for the selected range. The steep GWCC curves (Fig. 3) are consistent with the steep curves in Fig. 4. The hydraulic

conductivity of the geotextiles drops several orders of magnitude in the vicinity of 0.1 kPa. This is consistent with the geotextiles being hydraulically non-conductive at suctions greater than their water entry value (suction at residual saturation).

### 3. Model calibration and verification

Numerical simulations were carried out using the finite element program SVFlux v5.10 (SVFlux, 2004). The governing equation for transient water flow within unsaturated media follows that proposed by Richards (1931) and is described by Ho (2000) and Iryo and Rowe (2004) amongst many others. Numerical model monitoring points are illustrated on the schematic in Fig. 1. The program features a dynamic meshing algorithm which facilitates and optimizes mesh design. To ensure numerical stability using the steep GWCCs and associated unsaturated hydraulic conductivity curves, the PREFER\_STABILITY option was selected. The column was modelled as a two-dimensional domain 1.95 m in height and 10.2 cm wide subjected to a constant (10 cm) head boundary condition at the top and a free boundary at the bottom. A very permeable region was connected to the base of the infiltration column to model system response after the wetting front reached the bottom of the column. This detail was necessary to simulate the time delay as water fills the standpipe shown in Fig. 1. For models with sand and a geotextile, the geotextile was placed 0.75 m above the free water boundary (~ 1.20 m below the surface) matching the physical experiment.

Numerical monitoring points were located along one vertical line at 0.05 m intervals along the height of the numerical column, and a second set placed at the same location as the tensiometers and geotextile layer in the experiments (Fig. 1). The advantage of numerical experiments over physical experiments is that an essentially continuous temporal and spatial set of data can be captured along the height of the model.

As mentioned earlier, Iryo and Rowe (2003, 2004) also carried out numerical simulation of some of the column tests described here using a different commercially available finite element code. However, there are significant differences. In the current study all five tests were simulated as opposed to the control (sand only) test and the two tests with the nonwoven geotextile. Furthermore, different models for the GWCCs, SWCC and unsaturated hydraulic conductivity functions were used (i.e. van Genuchten (1980) and Mualem (1976) in the numerical modelling work by Iryo and Rowe, and Fredlund and Xing (1994) and Leong and Rahardjo (1997) in this study). The benefit of Fredlund and Xing (1994) model is that it provides the most generalized form of the SWCC and GWCC equation. Comparisons with conductivity probe response are also described in the current study which were not attempted by Iryo and Rowe (2003, 2004). Nevertheless, there are no significant qualitative differences between the two studies where predictions can be compared. However, there are some important quantitative differences. For example, Iryo and Rowe (2004) reduced both the hydraulic conductivity function as well as the maximum degree of saturation of the sand and geotextiles in order to match the physical results. Iryo and Rowe (2004) used their verified numerical model to quantify the effect of different soil types having saturated hydraulic conductivities that are greater than and less than that of the geotextile inclusion and to examine the influence of different boundary conditions. In the current study, the primary objective of the parametric analysis is to extend the database of 1-D physical column test results to a wider range of geotextile hydraulic conductivity and thickness (or permittivity) while keeping the calibrated sand properties and boundary conditions the same as those for the physical column tests. In summary, the earlier paper by Iryo and Rowe (2004) and the current study can be viewed as complimentary investigations.

Table 1  
Index (measured) and adjusted (modelled) parameters for sand.

Parameter	Index value	Adjusted value
Porosity	0.52	0.52
Saturated hydraulic conductivity, $K_{sat(sand)}$ (m/s)	$2.0 \times 10^{-3}$	$1.98 \times 10^{-3}$

**Table 2**  
Index (measured) and adjusted (modelled) parameters for geotextiles.

Geotextile	Parameter	Index value		Adjusted value	
		New	Modified	New	Modified
Woven	Thickness, $t_g$ (mm)	1.8	1.8	1.8	1.8
	Porosity, $n_g$	0.72	0.64	0.72	0.64
	Permittivity, $\Psi$ ( $s^{-1}$ )	0.36	0.35	0.011	0.0078
	Saturated hydraulic conductivity, $K_{sat(geotextile)}$ (m/s)	$6.6 \times 10^{-4}$	$6.4 \times 10^{-4}$	$2.0 \times 10^{-5}$	$1.4 \times 10^{-5}$
Nonwoven	Thickness, $t_g$ (mm)	3.8	3.8	3.8	3.8
	Porosity, $n_g$	0.86	0.32	0.86	0.32
	Permittivity, $\Psi$ ( $s^{-1}$ )	0.38	0.13	0.053	0.0024
	Saturated hydraulic conductivity, $K_{sat(geotextile)}$ (m/s)	$1.4 \times 10^{-3}$	$4.8 \times 10^{-4}$	$2.0 \times 10^{-4}$	$9.0 \times 10^{-6}$

### 3.1. Sand column

The calibration criteria for the sand column consisted of matching the tensiometer and conductivity probe data. The tensiometers provided measurements of negative and positive pore-water pressure in the area above and below the geotextile inclusion. The time when the water front passed the tensiometer elevation was interpreted as the maximum slope of the pore-water pressure data versus time plot. The conductivity probes indicated the time when the water front passed the elevation of the device by interpreting a change in voltage (Bathurst et al., 2007). In the numerical simulations volumetric water content, hydraulic conductivity and pore-water pressure were monitored at 0.05 m increments along the length of the column as well as at the same locations as the tensiometers.

Prior to initiating surface infiltration, the physical columns were drained to the free water boundary (Fig. 1). The average tensiometer measurement prior to infiltration was  $-1.1$  kPa (i.e. suction) and gravimetric water content was constant at 9–10%. In order to create these initial conditions in the numerical experiments an initial suction of 1.1 kPa was applied along the length of the column. This is consistent with results from Barbour and Yanful (1994) who found that suction increases were limited to the suction at the residual saturation level of granular soils in similar drained column tests.

Model calibration and verification was partly based on matching the water front progression in numerical and physical experiments with the latter interpreted from conductivity probe response. In the numerical experiments there was a large change in volumetric water content from an initial value of about 0.17 to about 0.52 that took place over approximately 4 s. A value of 0.35 was selected as the value to identify the water front since this is the middle of the transition between unsaturated and saturated states and was also in agreement with peak changes in pore-water pressure at numerical monitoring points. However, it was found that for post-processing the 0.35-volumetric water content criterion was less ambiguous than using pore-water pressure predictions to locate the wetting front.

Numerical and physical results for the column with sand only are shown in Fig. 5. Fig. 5a shows the pore-pressure response at selected tensiometer locations. Fig. 5b shows pore-water pressure

profiles at selected times and Fig. 5c shows the wetting front progression with time.

The tensiometer results show a reasonably good fit between the physical and numerical data. Initially pore-water pressure is an average of  $-1.1$  kPa for the tensiometer monitoring points shown in Fig. 5a and the vertical profile of pore-water pressure along the column at  $t = 0$  s shown in Fig. 5b. As the water front passes a monitoring point, pore-water pressure increases and approaches 0 kPa. Once the free water boundary is reached at 256 s, pore-water pressures at the monitoring points increase up to hydrostatic pressure. The curved portions of the curve from 0 kPa to a hydrostatic distribution are the result of the water filling up the full-height standpipe shown in Fig. 1. The numerical simulations allow the entire pore-water response history of the column to be tracked for the duration of the test. Initially the entire column is at  $-1.1$  kPa pressure. As the water front tracks downward from the surface, a sharp drop in suction is observed at the water front. At locations where pore-water pressure was measured by the tensiometers there is good agreement between the selected results shown. Results are plotted in Fig. 5b until the water front reaches the free water boundary.

The water front progression plot (Fig. 5c) shows that the slopes of the numerical and physical results agree well but the experimental results fall to the right. This is likely due to: (a) differences in initial near-surface hydraulic behaviour between numerical and the physical models; (b) the time interval of 6 s used in the physical tests, and; (c) equilibration response time in the tensiometers (Bathurst et al., 2007). The rate of water front progression was found to be very sensitive to the magnitude of saturated hydraulic conductivity assumed in the numerical simulations. The best prediction is shown in Fig. 5c and was achieved by assuming  $K_{sat(sand)} = 1.98 \times 10^{-3}$  m/s versus the index value of  $K_{sat(sand)} = 2.0 \times 10^{-3}$  m/s (Table 1). The difference in these two values is well within experimental error using laboratory hydraulic conductivity testing. However, since the lower value gave detectable better agreement, this slightly reduced saturated hydraulic conductivity value was used in all sand-geotextile column simulations. For steady state conditions described later in the paper, differences in predicted maximum ponding head using these two saturated hydraulic conductivity values are negligible.

### 3.2. Sand-geotextile columns

A similar modelling methodology was used in the sand columns that included a geotextile inclusion. The sand parameters were applied to the column above and below the geotextile. The parameters for the GWCC (shown in Table 2, Fig. 3) were used in the model domain representing the geotextile. The goal of this modelling procedure was to match the measured ponding pressure by tensiometers as well as the shape of the progressing water front. In each of the models, a reduction of the geotextile saturated

**Table 3**  
Fredlund and Xing (1994) fitting parameters for characteristic curves.

Parameter	Sand	New geotextile		Modified geotextile	
		Woven	Nonwoven	Woven	Nonwoven
$a$ (kPa)	0.70	0.1	0.07	0.22	0.06
$n$	19.2	6.00	7.00	1.90	6.64
$m$	0.57	3.00	0.80	3.50	0.83
$\Psi_r$ (kPa)	5.00	5.00	0.14	0.43	5.17

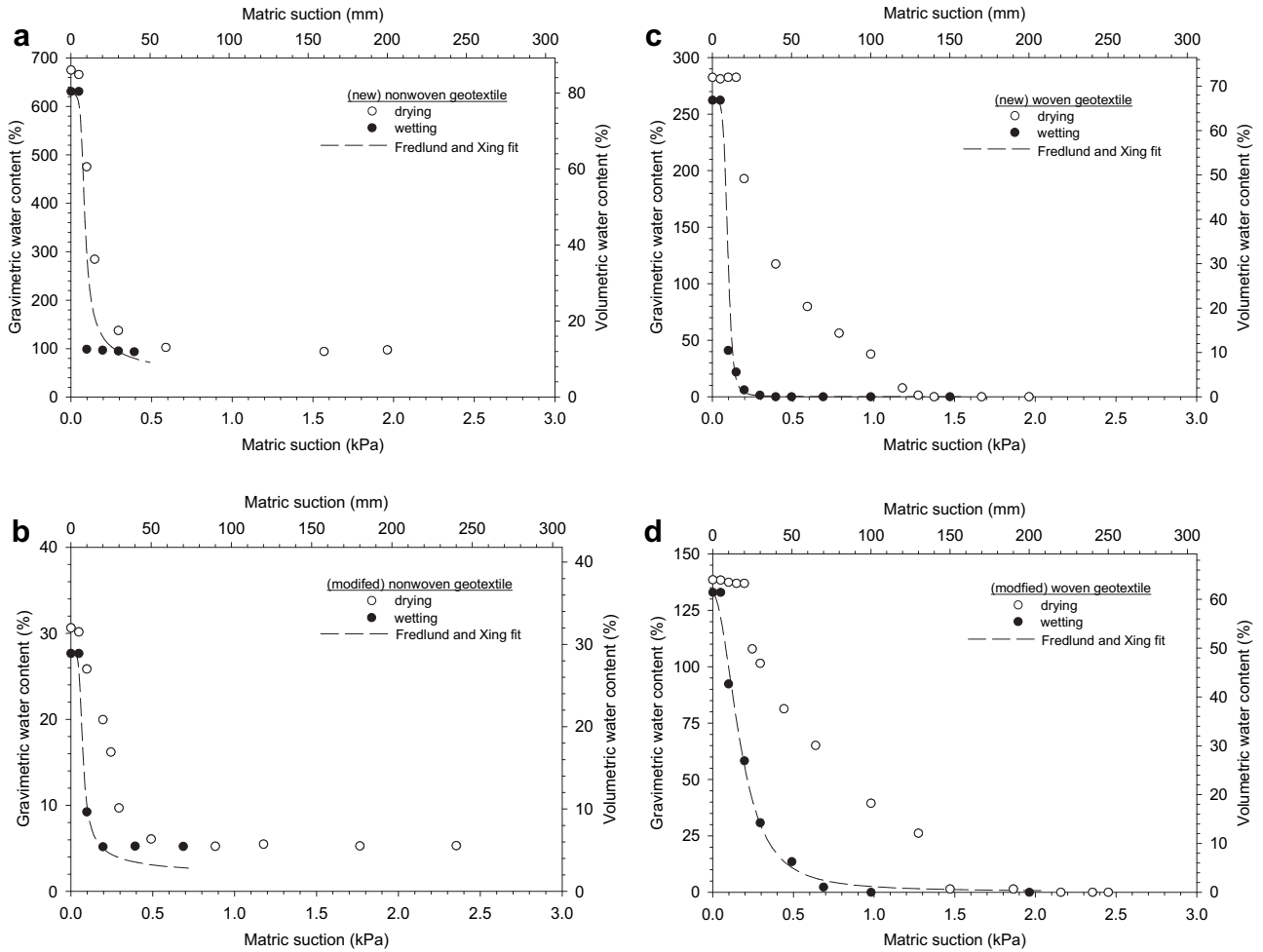


Fig. 3. Geotextile–water characteristic curves for new and modified geotextiles using Fredlund and Xing (1994). (a) new-nonwoven geotextile, (b) modified-nonwoven geotextile, (c) new-woven geotextile, (d) modified-woven geotextile.

hydraulic conductivity was required in order to model the measured ponding pressure and water front progression. The calibrated results for the four sand columns with geotextile inclusions are shown in Figs. 6–9. The column with the modified-

nonwoven geotextile is discussed in detail since this test generated the largest ponding response although qualitatively similar behaviour was observed in the other geotextile–sand tests.

The reasons for and the magnitude of parameter adjustments are described here. The measured thickness values and saturated hydraulic conductivity of the geotextiles were first used in the column test simulations. However, this resulted in negligible ponding and little change in the rate of water front advance below the geotextile as was observed in the physical testing. In order to predict the measured ponding pressures the hydraulic conductivity function was reduced by about two orders of magnitude for each geotextile (the adjusted values are given in Table 2 and plotted in Figs. 10 and 11). The reason for the required reduction in conductivity is intrusion of sand particles into the geotextile following placement in the column. The permittivity tests were performed in-isolation (ASTM D4491, 2004) without soil surrounding the geotextile and are therefore upper bound values. A similar corresponding reduction in geotextile saturated hydraulic conductivity has been reported in earlier simulation attempts of the RMC column tests by Ho (2000) and Iryo and Rowe (2004) to achieve a closer match with experimental results. The reduction in saturated hydraulic conductivity required to achieve the same ponding pressure shifts the entire hydraulic conductivity function downward (Fig. 4). The magnitude of reduction for  $K_{sat(geotextile)}$  ranges from 86% to 98% and increases with decreasing saturated hydraulic conductivity (Figs. 10 and 11).

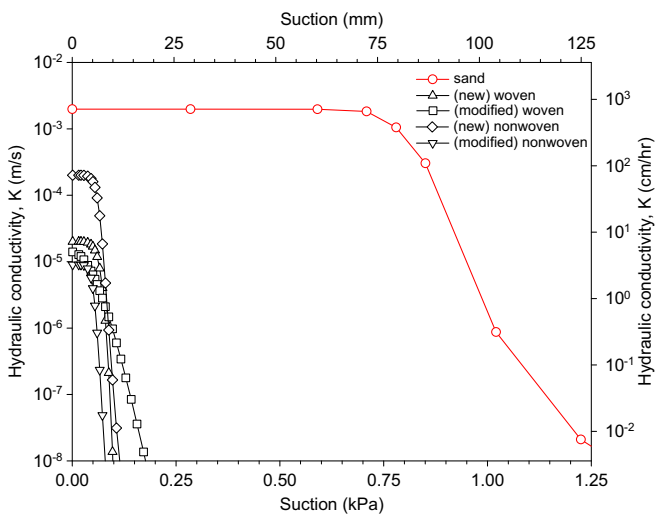


Fig. 4. Unsaturated hydraulic conductivity versus matric suction using functions from Leong and Rahardjo (1997).

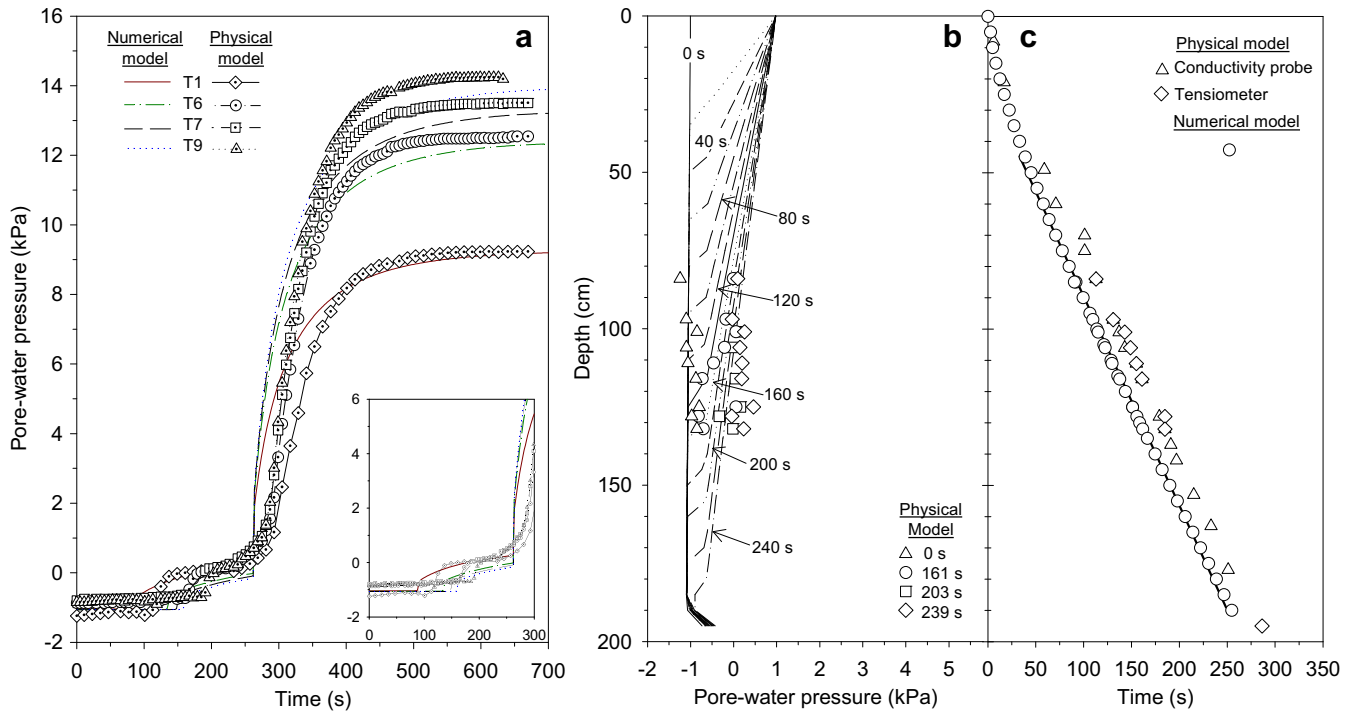


Fig. 5. Sand (only) column—numerical and physical test results: (a) pore-water pressure versus time, (b) pore-pressure profiles at selected times, and (c) water front progression versus time.

Calibrated results from the sand modified-nonwoven column are plotted in Fig. 6. As shown in Fig. 6a, the predicted pore-water pressures are consistent with measured values from 0 to 80 s. When the water front passes the T1 monitoring point, the pore-water pressure jumps and approaches 0 kPa. When the water front

reaches the modified-nonwoven geotextile at  $t = 141$  s, a second jump in pore-water pressure is recorded since an elevated ponding pressure is required to push the water through the geotextile. In the numerical simulation the jump occurs over less than 1 s compared with 40–50 s in the physical tests. This is due to compression of the

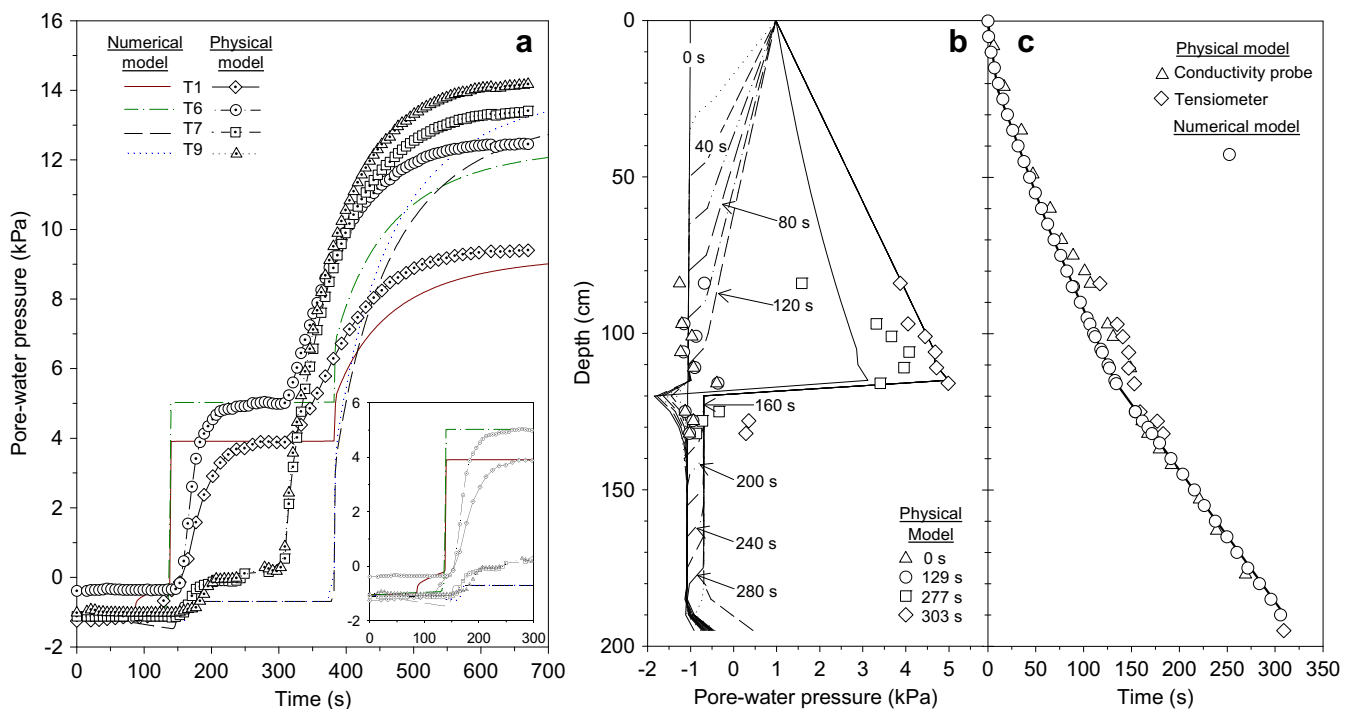


Fig. 6. Sand modified-nonwoven geotextile column—numerical and physical test results: (a) pore-water pressure versus time, (b) pore-pressure profiles at selected times, and (c) water front progression versus time.

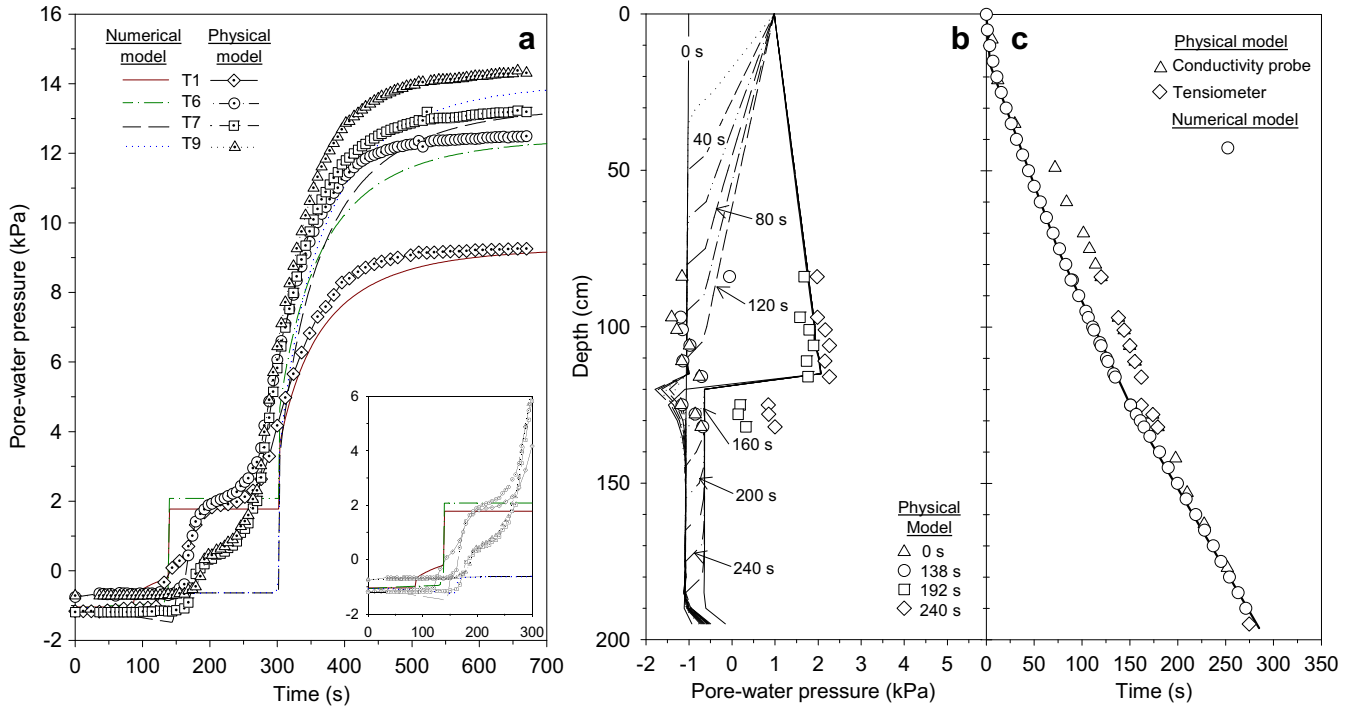


Fig. 7. Sand modified-woven geotextile column—numerical and physical test results: (a) pore-water pressure versus time, (b) pore-pressure profiles at selected times, and (c) water front progression versus time.

air phase within the soil in the physical experiments as well as possible small delays in response time of the tensiometer devices (Bathurst et al., 2007). Similar initial jumps are noted at the monitoring points below the geotextile; thereafter, pore-water pressure remains constant until the water front reaches the free

water boundary. At this stage the standpipe fills up and the pore-water pressure regime approaches hydrostatic conditions.

The entire pore-water pressure regime for the sand modified-nonwoven geotextile column is shown in Fig. 6b. Initially the entire column is at  $-1.1$  kPa pressure. At locations where tensiometer

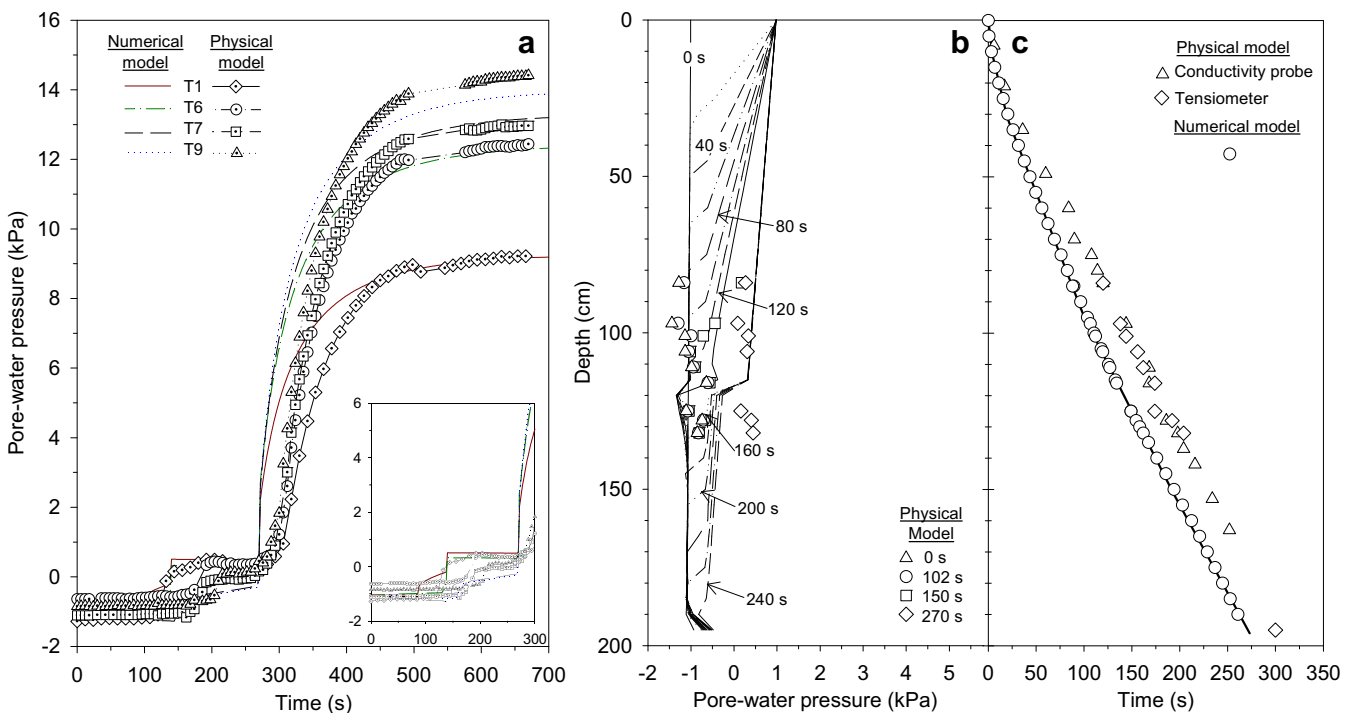


Fig. 8. Sand new-nonwoven geotextile column—numerical and physical test results: (a) pore-water pressure versus time, (b) pore-pressure profiles at selected times, and (c) water front progression versus time.

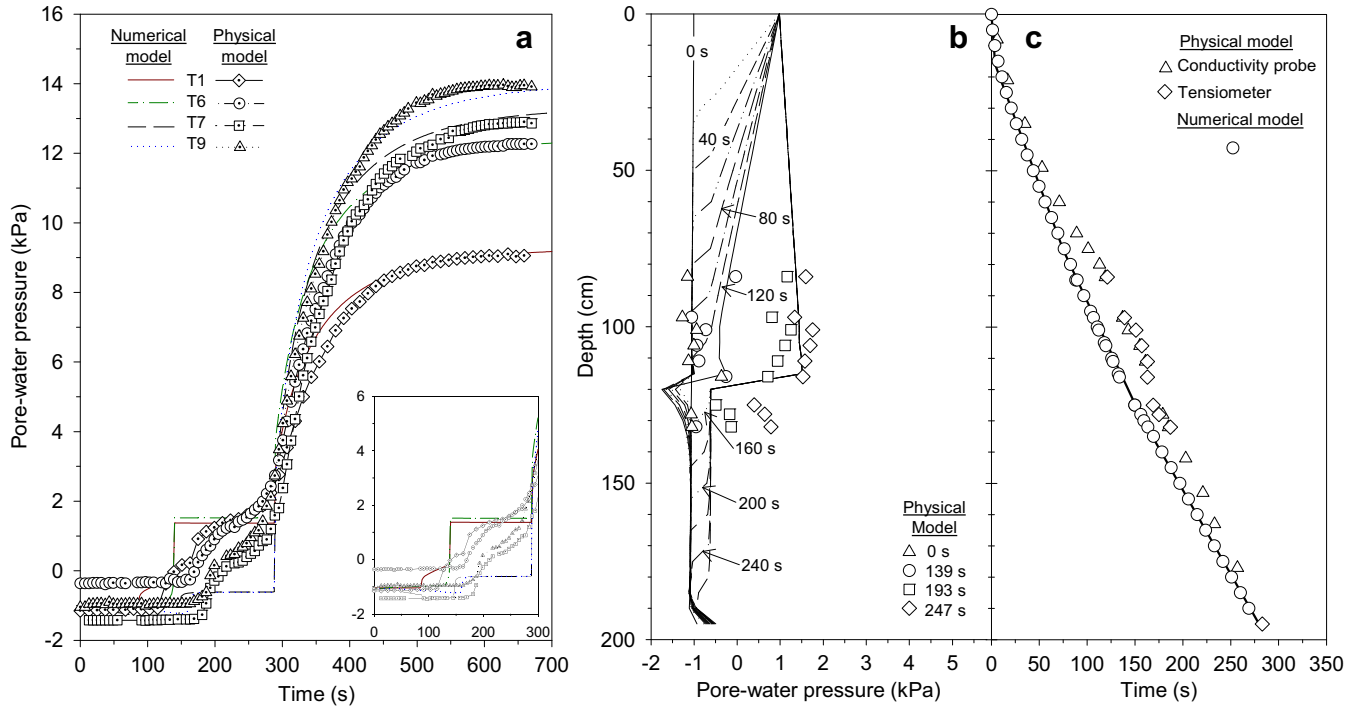


Fig. 9. Sand new-woven geotextile column—numerical and physical test results: (a) pore-water pressure versus time, (b) pore-pressure profiles at selected times, and (c) water front progression versus time.

readings were taken, there is judged to be reasonably good agreement between predicted and measured values as the water front progresses downward. When the water front reaches the geotextile the water mounds to a pressure head greater than the applied 10 cm head at the surface in order to push the water through the geotextile. Finally the water front continues towards the free water

boundary. However, the rate of advance is less than that for the water above the geotextile (e.g. compare vertical distance between 40 s increment pore-water isochrones).

The progression of the water front is plotted in Fig. 6c. Good agreement is observed between the numerical and physical results with some delay due to the reasons explained above. As the water front progresses downward from the surface it reaches a constant slope above the geotextile. At the geotextile layer ponding pressure develops and a change in slope of the water front progression curve is observed. This is in contrast to the sand-only column (Fig. 5b) where a constant slope was observed along the entire flow length. The reason for the change in slope is due to the ‘bottleneck’

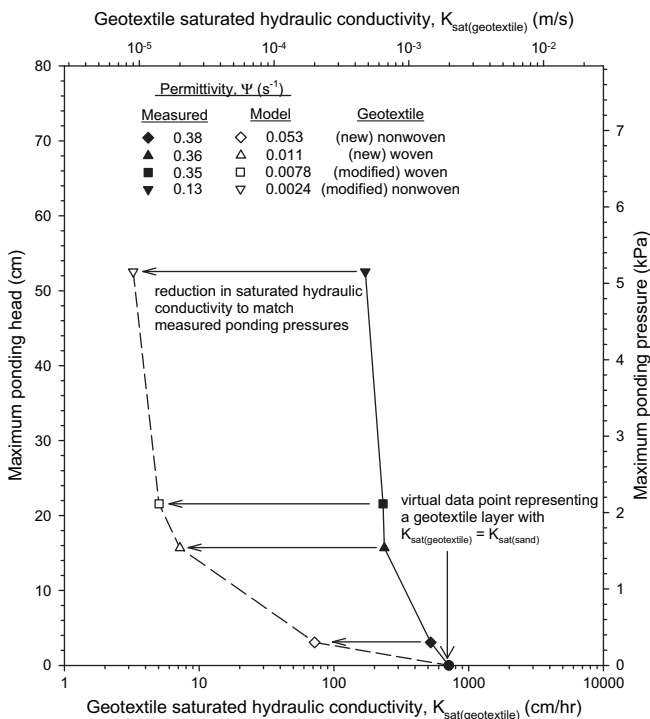


Fig. 10. Index (measured) and adjusted (modelled) geotextile saturated hydraulic conductivity versus ponding head.

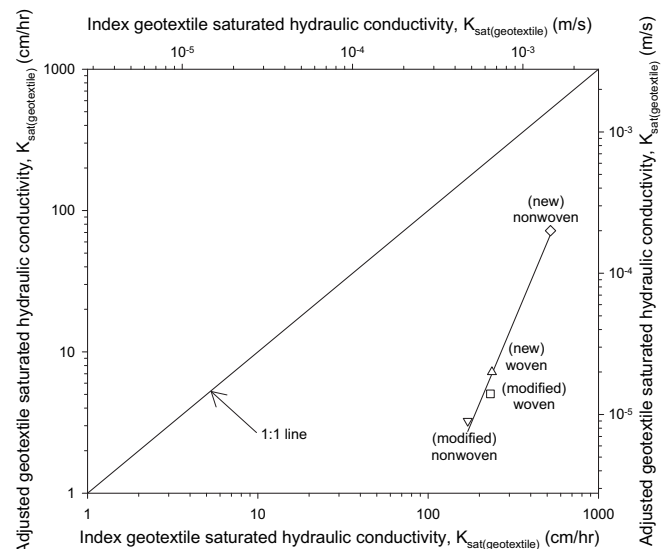


Fig. 11. Index and adjusted values of geotextile saturated hydraulic conductivity.

provided by the geotextile due to its lower saturated hydraulic conductivity compared with the surrounding soil (Fig. 4).

Similar calibration procedures and results were found for the other three tests shown in Figs. 7–9. The hydraulic conductivity values were reduced for all geotextiles. In each case a reasonably good fit was found between numerical and physical tests for the slopes of the water front progression curves and ponding pressures.

A summary of the water front progression for the five columns is shown in Fig. 12. Above the geotextile inclusion the five models show similar water front progression. The water front initially advances relatively quickly and follows a concave up pattern and then approaches a constant slope. For the models with a geotextile inclusion, an abrupt change in slope occurs at the location of the geotextile (time = 141 s). Below this elevation, the water front advances at a slower rate (gentler slope) as the water has to be pushed through the geotextile inclusion which has a lower saturated hydraulic conductivity (Fig. 4). The rate at which the water front advances is a function of the saturated conductivity and permittivity of the geotextile. The modified-nonwoven geotextile has the lowest hydraulic conductivity and consequently the slowest progression of the water front below the inclusion. The modified-woven, new-woven and new-nonwoven geotextiles have increasing conductivities and permittivities (in this order) and show reduced impact on the water front progression compared with the sand-only model.

In addition to the water front progression delay observed in the area around the inclusion, the hydraulic gradient around the geotextile is also a function of the saturated permittivity of the geotextile as shown in Fig. 13. Here, head loss between two tensiometer locations normalized to the distance between the tensiometers is plotted versus time. The two locations selected are between tensiometers T6 and T7 (closest to the inclusion) and T5 and T8 (farther from the inclusion). Similar observations and gradient magnitudes were reported for the physical results by Bathurst et al. (2009). Near the geotextile (Fig. 13a) high downward

gradients are required to push water through the geotextile which acts as a restriction in the flow system. Again the gradient is a function of the permittivity of the geotextile with the lowest permittivity requiring the largest gradient. Farther away from the geotextile (Fig. 13b) the gradients are not as pronounced but the same qualitative effect is observed.

4. Parametric study

The calibrated numerical model described above was used to investigate the influence of a wider range of geotextile saturated hydraulic conductivity and thickness (or permittivity), soil saturated hydraulic conductivity and thickness and surface boundary condition on the 1-D hydraulic response of soil–geotextile columns. An analytical model was also derived to predict ponding above the geotextile using steady state flow assumptions. Table 4 provides a summary of the range of values used in the parametric study.

4.1. Analytical model

The analytical model considers the maximum ponding head at the top of the geotextile before the water front reaches the bottom of the column. In Fig. 6 this corresponds to the time between 160 s and 280 s for the sand modified-nonwoven geotextile column. The pressure head and total head distributions during this stage are illustrated in Fig. 14. The model input parameters are depth of water at the surface ( $h_w$ ), thickness of soil or burial depth of the geotextile ( $t_s$ ), geotextile thickness ( $t_g$ ), and pressure head at the bottom surface of the geotextile ( $h_b$ ). The soil and geotextile are assumed to have constant hydraulic conductivities and the pressure head below the geotextile ( $h_b$ ) is assumed to be constant; hence, the ponding head can be derived for the case of two-layer saturated porous media subject to one-dimensional steady state flow. The closed-form solution is:

$$h_p = \frac{h_w + t_s + t_g - h_b}{\frac{\psi_g t_s}{K_s} + 1} + h_b - t_g \tag{4}$$

The following assumptions can be made to simplify this equation without introducing significant errors: (a)  $h_b$  is assumed to be zero, and (b) geotextile thickness  $t_g$  is negligible compared to the height of soil above the geotextile ( $t_s$ ). The first assumption is reasonable since the four physical tests described in this paper recorded very small values of  $h_b$  that varied from –4.1 cm to –6.4 cm (–0.4 kPa to –0.63 kPa). Ignoring the negative head in the above formulation leads to slightly higher ponding heads which is conservative (safe) for design. There is no practical prediction error by setting  $t_g = 0$ . The simplified analytical model can then be conveniently normalized by dividing the ponding head by the thickness of the soil plus depth of water at the surface. The resulting simplified equation is:

$$\frac{h_p}{h_w + t_s} = \frac{1}{\frac{\psi_s}{\psi_s} + 1} \tag{5}$$

where  $\psi_s = K_s t_s$  is called soil permittivity in this paper but is often called vertical conductance or vertical leakance in hydrogeology terminology. In the limit of geotextile hydraulic conductivity (or permittivity) equal to zero (impermeable hydraulic barrier), the ponding head above the geotextile is hydrostatic ( $h_p = h_w + t_s$ ). As geotextile hydraulic conductivity decreases (the geotextile becomes more permeable) the ponding head decreases. One difference between the two equations is that at higher permittivities, Equation (4) predicts a negative head above the geotextile. Very small negative heads were predicted in some numerical

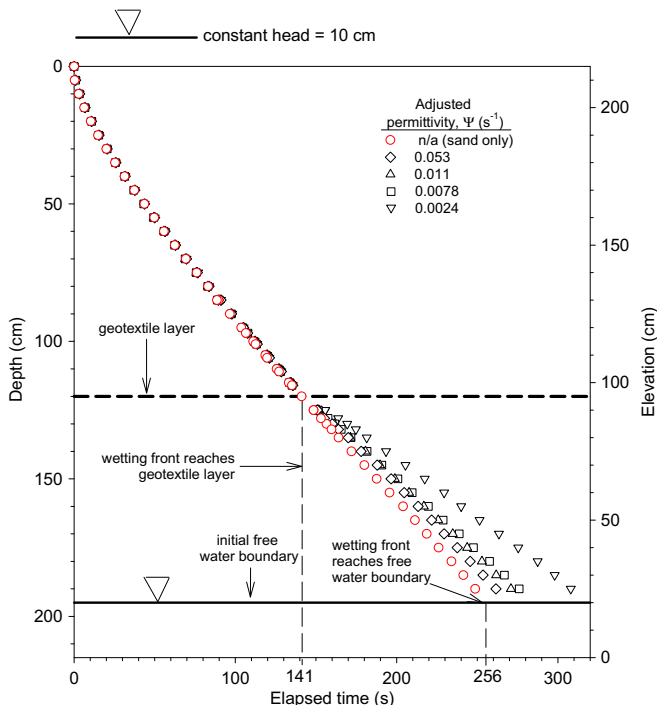


Fig. 12. Wetting front comparison for calibration models.

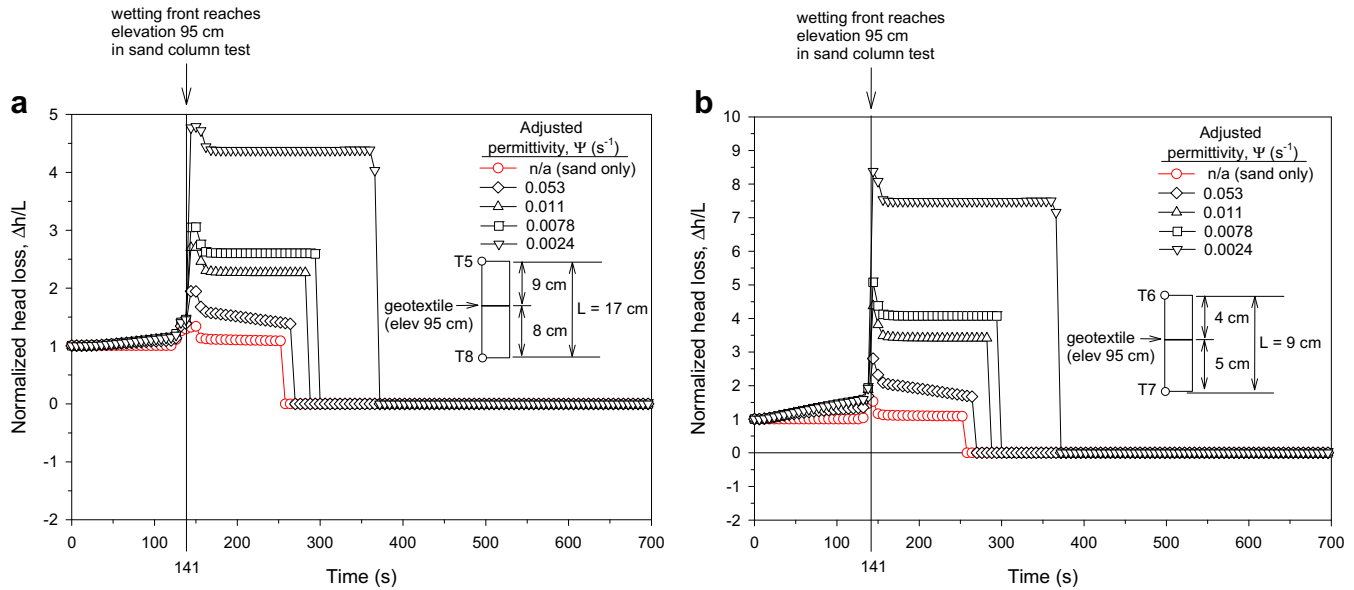


Fig. 13. Normalized head loss across the geotextile location of the sand and sand-geotextile column models with time. (a) between tensiometer monitoring points T5 and T8 ( $L = 17$  cm) (b) between tensiometer monitoring points T6 and T7 ( $L = 9$  cm).

parametric study cases. Comparisons between the results of numerical simulations and predicted values using Equation (5) are presented later.

#### 4.2. Influence of GWCC

The GWCCs for the new and modified geotextiles (Fig. 3) are very steep with transition suction ranges measured in millimetres to a few centimetres and air entry values of 5–10 mm suction. The influence of the GWCC on infiltration behaviour was assumed to be small because of the small geotextile thickness and steep GWCC. However, the influence of the GWCC on hydraulic response warrants further investigation. The Fredlund and Xing (1994) 'a' parameter was varied to determine its influence on the ponding head (pressure) measured above the geotextile. The 'a' parameter is related to the air entry value of the geotextile but strictly speaking it is the upper inflection point of the GWCC function (Equation (1a)). As shown in Fig. 3, modification of the geotextiles resulted in changing the air entry value and shape of the GWCC. However, in order to limit the scope of the parametric study only the influence of the magnitude of parameter "a" was investigated.

Maximum ponding head is defined as the pressure head measured at the upper surface of the geotextile. In the calibration test results with a geotextile inclusion (Figs. 6–9) the pore-water pressure profile was a straight line from the 10 cm of head applied at

the surface to the monitoring point just above the geotextile (Fig. 1). To calculate the ponding pressure at the surface of the geotextile, this line was extended to the elevation of the top of the geotextile.

The influence of the 'a' parameter on the numerical results for models with geotextile inclusions is plotted in Fig. 15. The solid symbols represent numerical parametric results using values of 'a' that vary from the best-fit calibration models (open symbols). The 'a' parameter was varied from 0.06 kPa to 2.0 kPa as reported in Table 4. This range was selected because it bounds the initial suction in the column as well as the anticipated range of 'a' values for various geotextiles (Bathurst et al., 2007; Nahlawi et al., 2007; Krisdani et al., 2006). Increasing 'a' simply shifts the entire GWCC and unsaturated hydraulic conductivity to the right (Figs. 3 and 4). Since only wetting conditions (decreasing suction) apply for the models, shifting the unsaturated hydraulic conductivity function past the initial suction applied to the geotextile results in the hydraulic conductivity remaining constant for the entire model run. This removes the effect of the reduction in hydraulic conductivity of the geotextile due to de-saturation. Despite the two orders of magnitude variation, little influence was observed on the resulting ponding head (Fig. 15). The rate of progression of the water front was also not significantly altered by varying this parameter. Because the GWCCs for the geotextiles in this study are very steep, the 'a' parameter essentially defines the suction value during wetting at which the geotextile switches from being non-conductive to having maximum hydraulic conductivity (saturated permeability). Since the GWCCs are so steep it may not be surprising that the magnitude of parameter 'a' has little effect on the hydraulic response of the sand-geotextile columns in this numerical investigation.

Table 4  
Range of parameters used in numerical parametric study.

Parameter	Range
Fredlund and Xing (1994) 'a' parameter (kPa)	0.06–2.0
Geotextile hydraulic conductivity, $K_{sat(geotextile)}$ (m/s)	$2 \times 10^{-3}$ – $1 \times 10^{-6}$
Geotextile thickness, $t_g$ (mm)	0.8–9.8
Soil hydraulic conductivity, $K_{sat(soil)}$ (m/s)	$2 \times 10^{-5}$ – $2 \times 10^{-2}$
Geotextile placement depth, $t_s$ (m)	0.6, 1.2, 1.8
Ponding height (m)	0.1, 0.25
Ratio of hydraulic conductivity, $K_{sat(soil)}/K_{sat(geotextile)}$	0.02–20 000
Geotextile permittivity, $\Psi_g$ ( $s^{-1}$ )	$1 \times 10^{-6}$ – $5.5 \times 10^{-1}$
Ratio of soil permittivity to geotextile permittivity, $\Psi_s/\Psi_g$	$1 \times 10^{-4}$ – $2.0 \times 10^2$

#### 4.3. Geotextile saturated hydraulic conductivity, $K_{sat(geotextile)}$ and thickness, $t_g$

To expand the database of numerical simulation results using the reference column tests, the saturated hydraulic conductivity of the four geotextiles was first varied from  $2 \times 10^{-3}$  m/s to  $1 \times 10^{-6}$  m/s (e.g.  $K_{sat(sand)}/K_{sat(geotextile)}$  varied from 1 to 1980) while holding geotextile thickness and the column configuration

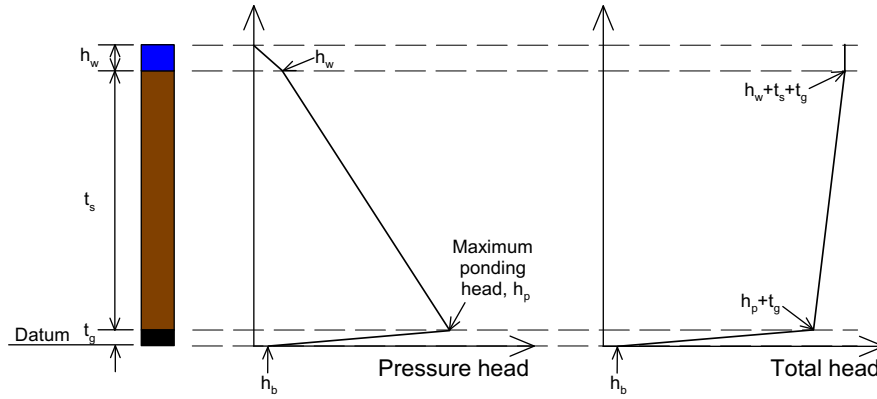


Fig. 14. Details of analytical model to predict maximum ponding head above geotextile.

constant. Next the saturated hydraulic ratio was kept constant and the geotextile thickness varied between 0.8 mm and 9.8 mm.

Results are presented in Fig. 16 solid symbols are from the four physical tests using corrected  $K_{sat(geotextile)}$  values and the open symbols from the numerical parametric study. The continuous lines were calculated using the analytical model described above (Equation (5)). The data show that ponding pressure (or head) increases nonlinearly with decreasing geotextile conductivity (increasing  $K_{sat(sand)}/K_{sat(geotextile)}$ ) for each geotextile thickness. The analytical model results are in very good agreement with numerical results and the four physical test measurements.

The plots in Fig. 16 show that below a threshold value of  $K_{sat(sand)}/K_{sat(geotextile)}$ , ponding heads are very small or even slightly negative. This value is taken as  $K_{sat(sand)}/K_{sat(geotextile)} = 2$  for the models with 3.8 mm thick geotextiles and  $K_{sat(sand)}/K_{sat(geotextile)} = 6$  for the 1.8 mm thick geotextiles. At first, this result appears to conflict with the recommendation by Bathurst et al. (2009) to limit  $K_{sat(sand)}/K_{sat(geotextile)}$  to not more than 0.1 in order to prevent ponding. However, this recommendation was based on hydraulic conductivity ratios computed using the measured in-isolation values for the geotextiles. Recall that these values must be reduced by up to two orders of magnitude to match the physical column test results (adjusted values are shown in Table 2 and in Fig. 11). Recall also the strong influence of geotextile thickness on the numerical simulations and the practical limitations of measuring this parameter. Therefore, the earlier recommendation by the writers is still valid since designers will

only have available measured in-isolation hydraulic conductivity values. In critical applications, including cyclic flow conditions (e.g. coastal revetments) a ratio of 10 has been recommended (Holtz et al., 1997; Chen et al., 2008). What the current paper demonstrates is that to extend the database of physical tests first reported by Bathurst et al. (2009) using numerical simulations, the saturated hydraulic conductivities of the geotextiles determined from conventional laboratory tests must be reduced.

#### 4.4. Soil hydraulic conductivity, $K_{sat(soil)}$

To investigate the influence of the surrounding soil layers the hydraulic conductivity of the soil was varied from the baseline value of  $1.98 \times 10^{-3}$  m/s to values of  $2.0 \times 10^{-2}$  m/s and  $2.0 \times 10^{-5}$  m/s while holding the other variables constant including the soil SWCC. In fact, a change in hydraulic conductivity of these magnitudes would require a significant change in the particle-size

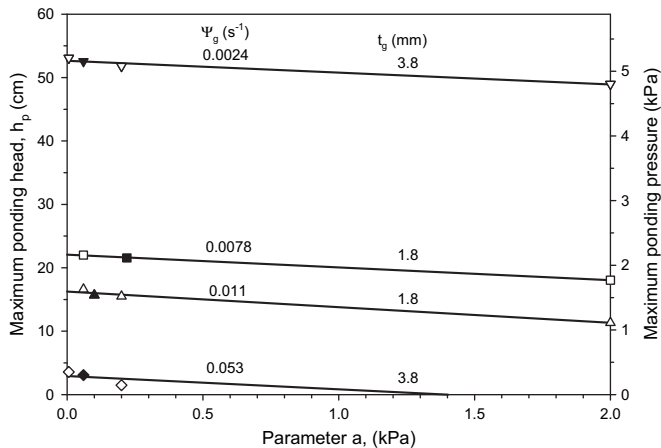


Fig. 15. Influence of Fredlund and Xing (1994) 'a' parameter on maximum ponding head. Notes: Solid symbols are from physical tests using corrected saturated hydraulic conductivity values for geotextiles; open symbols are results of numerical simulation.

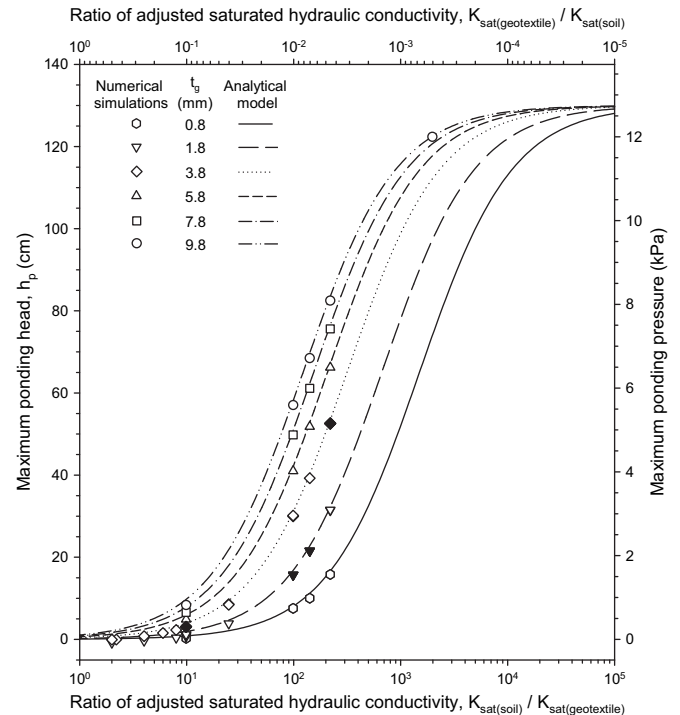


Fig. 16. Influence of geotextile thickness and hydraulic conductivity on maximum ponding head. Note: Solid symbols are from physical tests using corrected saturated hydraulic conductivity values for geotextiles.

distribution and a corresponding change in the SWCC. However, the goal of the parametric study was to investigate the influence of each parameter individually and hence the SWCC was not changed.

The results of the parametric study to investigate the influence of soil hydraulic conductivity are plotted in Fig. 17 as maximum ponding head versus adjusted geotextile permittivity plotted on a log scale. The agreement between the results of numerical simulations and analytical model (Equation (5)) is judged to be very good. The results show that as geotextile permittivity decreases, ponding head increases nonlinearly up to the hydrostatic ponding head for this configuration ( $t_s + h_w = 130$  cm). The data show that it is the combination of geotextile permittivity and soil hydraulic conductivity that governs the maximum ponding head above a geotextile placed at a finite depth.

4.5. Soil layer thickness,  $t_s$  and height of surface water,  $h_w$

According to the analytical model introduced earlier, the total ponding potential is the total height of the surface water added to the thickness of the soil layer. The effects of soil layer thickness and depth of surface water are investigated here. In addition to the 1.2 m placement depth investigated thus far, geotextiles were simulated at depths of 0.6 m and 1.8 m. The combined condition of burial depth of 1.2 m and a water height of 0.25 m was also simulated. Fig. 18 shows that the ponding head increases as the ratio of soil hydraulic conductivity to geotextile permittivity increases. As the soil layer thickness increases, maximum ponding head increases for values of soil conductivity to geotextile permittivity ratio greater than (say) 0.3 m. The hydrostatic head also increases linearly with depth of surface water which can be seen by comparing the steady state (maximum) ponding values for the two cases with depth of geotextile  $t_s = 1.2$  m. As expected, the maximum possible ponding head is the hydrostatic value shown at the right end of each plot.

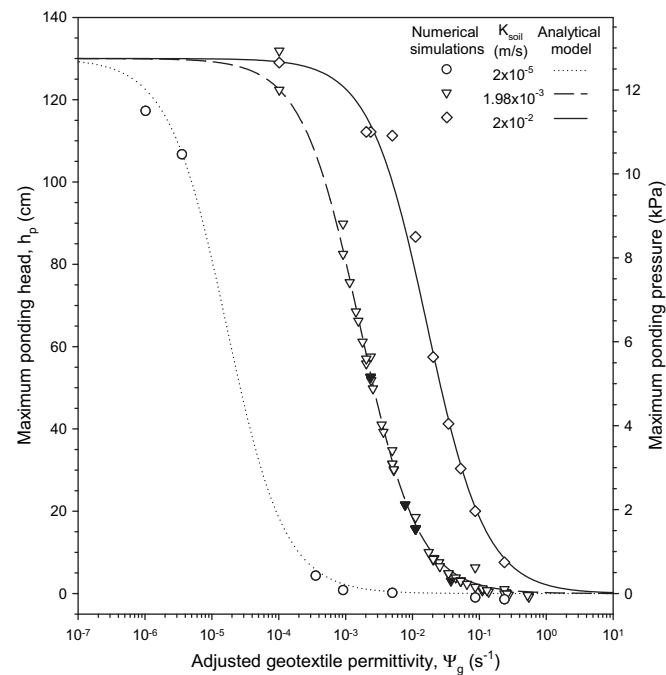


Fig. 17. Influence of soil hydraulic conductivity and geotextile permittivity on maximum ponding head. Note: Solid symbols are from physical tests using corrected saturated hydraulic conductivity values for geotextiles.

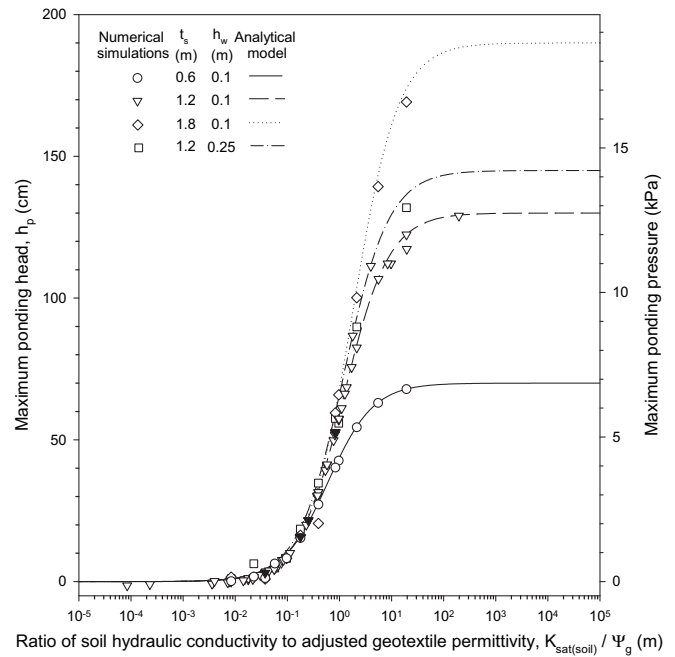


Fig. 18. Influence of depth of geotextile on ponding head. Note: Solid symbols are from physical tests using corrected saturated hydraulic conductivity values for geotextiles.

5. Design chart

The results of all numerical simulations can be collapsed onto a single curve representing the analytical model described by Equation (5) (Fig. 19). This figure can be used as a design chart to

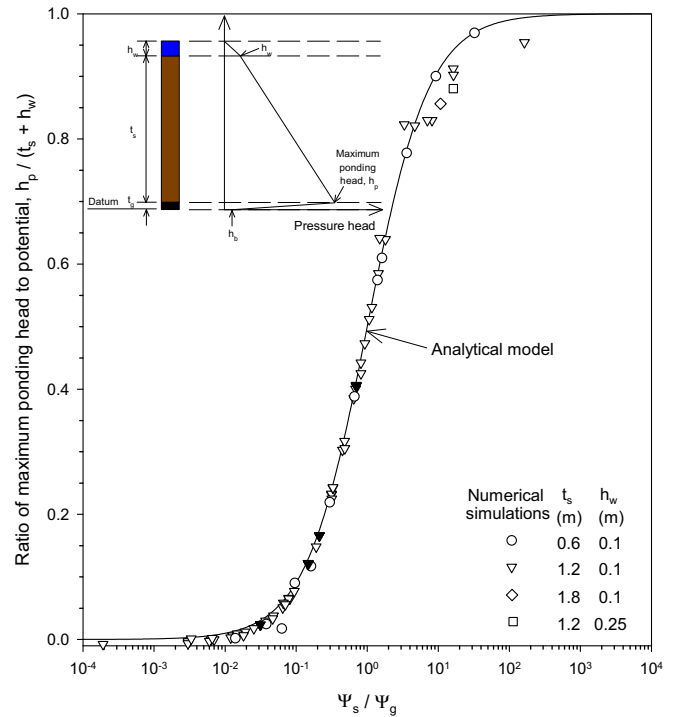


Fig. 19. Normalized design chart to predict maximum ponding head under saturated steady state flow conditions in the geotextile and cover soil. Note: Solid symbols are from physical tests using corrected saturated hydraulic conductivity values for geotextiles.

predict maximum ponding head above a geotextile for the 1-D conditions assumed in this investigation. Below a value of approximately  $\Psi_s/\Psi_g = 0.01$  (say), negligible ponding can be expected. At the other extreme, for  $\Psi_s/\Psi_g > 100$  (say), hydrostatic conditions are predicted provided the surface infiltration loading period is long enough.

The following steps are required to use Fig. 19 for design:

1. Perform in-isolation permittivity test (e.g. ASTM D4491, 2004) on candidate geotextile and compute the index saturated hydraulic conductivity,  $K_{\text{sat(geotextile)}}$ .
2. Perform normal compression test on geotextile to estimate its thickness ( $t_g$ ) under project-specific overburden pressure (e.g. ASTM D5199, 2004).
3. Reduce the laboratory  $K_{\text{sat(geotextile)}}$  value using Fig. 11 to account for soil intrusion.
4. Compute saturated hydraulic permittivity of the geotextile ( $\Psi_g$ ) using the adjusted  $K_{\text{sat(geotextile)}}$  value and compressed geotextile thickness ( $t_g$ ) (e.g. Equation (2)).
5. Compute the ratio ( $\Psi_s/\Psi_g$ ) and enter chart.

## 6. Discussion and conclusions

This paper presents the results of calibration of a numerical model and parametric analysis of surface water infiltration into initially unsaturated 1-D sand columns containing a geotextile inclusion.

A close fit to the measured GWCC using Fredlund and Xing (1994) unsaturated soil model was difficult to achieve in the steep transition zone. However, beyond a threshold steep slope value there was no influence on column test results. Furthermore, the parametric analysis of the geotextile properties showed that there was little influence of the location of the upper inflection point in the GWCC of the geotextiles that is quantified by parameter 'a' in Fredlund and Xing (1994) model. This is judged to be because the GWCCs for these materials are very steep. However, numerical results were sensitive to changes in the geotextile thickness, saturated hydraulic conductivity and associated permittivity.

Column test calibration models required a reduction of the geotextile hydraulic conductivity function of up to two orders of magnitude in order to match the measured ponding head and water front progression. The physical reason for the required reduction was ascribed to sand intrusion into the geotextile from the surrounding soil. This phenomenon was not captured by conventional laboratory permittivity tests. In the numerical calibration runs the ponding head and rate of water front progression were observed to vary with the magnitude of saturated hydraulic conductivity assumed for the geotextile inclusion.

The results of numerical modelling indicate that for each geotextile thickness there is a ratio of soil permittivity to geotextile permittivity value ( $\Psi_s/\Psi_g$ ) below which no ponding will occur. For the no ponding condition,  $\Psi_s/\Psi_g$  was required to be less than 0.01. Since saturated permeability and geotextile thickness are related, the critical permittivity to prevent ponding may be estimated using measured values that are reduced to account for soil intrusion and geotextile compression. The relationship between permittivity ratio and ponding head potential was found to be highly non-linear. A simple analytical model for ponding head was derived assuming a two-layer saturated porous media subject to one-dimensional steady state flow. The analytical results were shown to be in very good agreement with physical test results and results from a much broader numerical parametric study. Finally, a design methodology to predict ponding pressures in 1-D soil-

geotextile systems is proposed based on the simple analytical model.

## Acknowledgements

The work described in this paper was supported by grants awarded to the authors by the Natural Sciences and Engineering Research Council of Canada, the Academic Research Program at RMC, the Department of National Defence (Canada) and British Petroleum (formerly Amoco).

## Notation

Basic SI units are given in parentheses.

$a$	fitting parameter (Pa)
$e$	2.718 (dimensionless)
$C(\Psi)$	correction function (dimensionless)
$h$	matric suction head (m)
$h_w$	head (depth) of water at surface of column (m)
$h_p$	maximum ponding head (m)
$K_{\text{sat}}$	saturated hydraulic conductivity (m/s)
$K(\Psi)$	unsaturated hydraulic conductivity
$K_{\text{sat(geotextile)}}$	saturated hydraulic conductivity of geotextile (m/s)
$K_{\text{sat(sand)}}$	saturated hydraulic conductivity of sand (m/s)
$K_{\text{sat(soil)}}$	saturated hydraulic conductivity of soil (m/s)
$L$	length (m)
$n, m$	fitting parameters (dimensionless)
$n_g$	porosity of geotextile (dimensionless)
$p$	fitting parameter (dimensionless)
$t_g$	thickness of geotextile (m)
$t_s$	thickness of soil above geotextile or placement depth of geotextile (m)
$\Delta h$	head loss (m)
$\Psi$	suction (Pa)
$\Psi_r$	fitting parameter (Pa)
$\Psi_g$	geotextile saturated permittivity ( $s^{-1}$ )
$\Psi_s$	soil saturated permittivity ( $s^{-1}$ )
$\theta$	water content (dimensionless)
$\theta_s$	saturated water content (dimensionless)

## Abbreviations

GWCC	gravimetric water content (dimensionless)
GWCC	geotextile–water characteristic curve
SWCC	soil–water characteristic curve

## References

- ASTM D4491, 2004. Standard Test Method for Water Permeability of Geotextiles by Permittivity. American Society for Testing and Materials, West Conshohocken, PA, USA.
- ASTM D5199, 2004. Standard Test Method for Measuring the Nominal Thickness of Geosynthetics. American Society for Testing and Materials, West Conshohocken, PA, USA.
- ASTM D5493, 2003. Standard Test Method for Permittivity of Geotextiles Under Load. American Society for Testing and Materials, West Conshohocken, PA, USA.
- Barbour, S.L., Yanful, E.K., 1994. A column study of static nonequilibrium fluid pressure in sand during prolonged drainage. Canadian Geotechnical Journal 31 (2), 299–303.
- Bathurst, R.J., Ho, A.F., Siemens, G., 2007. A column apparatus for investigation of 1-D unsaturated-saturated response of sand-geotextile systems. ASTM Geotechnical Testing Journal 30 (6), 433–441.
- Bathurst, R.J., Siemens, G.A., Ho, A.F., 2009. Experimental investigation of infiltration ponding in one-dimensional sand-geotextile columns. Geosynthetics International 16 (3), 158–172.
- Bouazza, A., Zornberg, J.G., McCartney, J.S., Nahlawi, H., 2006. Significance of unsaturated behaviour of geotextiles in earthen structures. Australian Geomechanics 41 (3), 133–142.
- Canadian Foundation Engineering Manual, 2006, fourth ed. Canadian Geotechnical Society, Richmond, B.C. Canada, 488 p.

- Cartaud, F., Touze-Foltz, N., Duval, Y., 2005. Experimental investigation of the influence of a geotextile beneath the geomembrane in a composite liner on leakage through a hole in the geomembrane. *Geotextiles and Geomembranes* 23 (2), 117–143.
- Chen, R.-H., Ho, C.-C., Hsu, C.-Y., 2008. The effect of fine soil content on the filtration characteristics of geotextile under cyclic flows. *Geosynthetics International* 15 (2), 1–12.
- Fredlund, D.G., Xing, A., 1994. Equations for the soil-water characteristics curve. *Canadian Geotechnical Journal* 31 (4), 521–532.
- Garcia, E.F., Gallage, C.P.K., Uchimura, T., 2007. Function of permeable geosynthetics in unsaturated embankments subjected to rainfall infiltration. *Geosynthetics International* 14 (2), 89–99.
- van Genuchten, M.Th., 1980. A closed-form equation for predicting the hydraulic conductivity of unsaturated soils. *Soil Science Society of America Journal* 44 (5), 892–898.
- Ho, A.F., 2000. Experimental and numerical investigation of infiltration ponding in one-dimensional sand-geotextile columns, MSc thesis. Queen's University, Kingston, Ontario, 212 pp.
- Holtz, R.D., Christopher, B.R., Ryan, R.B., 1997. *Geosynthetic Engineering*. BiTech Publishers, Richmond, (British Columbia, Canada).
- Iryo, T., Rowe, R.K., 2003. On the hydraulic behavior of unsaturated nonwoven geotextiles. *Geotextiles and Geomembranes* 21 (2), 381–404.
- Iryo, T., Rowe, R.K., 2004. Numerical study of infiltration into a soil-geotextile column. *Geosynthetics International* 11 (5), 377–389.
- Iryo, T., Rowe, R.K., 2005a. Hydraulic behaviour of soil-geocomposite layers in slopes. *Geosynthetics International* 12 (3), 145–155.
- Iryo, T., Rowe, R.K., 2005b. Infiltration into an embankment reinforced by nonwoven geotextiles. *Canadian Geotechnical Journal* 42 (4), 1145–1159.
- Knight, M.A., Kotha, S.M., 2001. Measurement of geotextile-water characteristic curves using a controlled outflow capillary pressure cell. *Geosynthetics International* 8 (3), 271–282.
- Koerner, R.M., 2005. In: *Designing with Geosynthetics*, fifth ed. Prentice Hall, Upper Saddle River, New Jersey, USA.
- Krisdani, H., Rahardjo, H., Leong, E.C., 2006. Experimental study of 1-D capillary barrier model using geosynthetic material as the coarse-grained layer, In: proceedings of the fourth International Conference on Unsaturated Soils, Carefree, Arizona, USA, pp. 1683–94.
- Krisdani, H., Rahardjo, H., Leong, E.C., 2008. Measurement of geotextile-water characteristic curve using capillary rise principle. *Geosynthetics International* 15 (2), 86–94.
- Lafleur, J., Lebeau, M., Faure, Y.H., Savard, Y., Kehila, Y., 2000. Influence of matric suction on the drainage performance of polyester geotextiles, In: proceedings of the 53rd Annual Conference of the Canadian Geotechnical Society, Montreal, Quebec, CANADA, pp. 1115–22.
- Leong, E.C., Rahardjo, H., 1997. Permeability functions for unsaturated soils. *Journal of Geotechnical and Geoenvironmental Engineering* 123 (12), 1118–1126.
- Mualem, Y., 1976. A new model for predicting the hydraulic conductivity of unsaturated porous media. *Water Resources Research* 12 (3), 513–522.
- Nahlawi, H., Bouazza, A., Kodikara, J., 2007. Characterisation of geotextiles water retention using a modified capillary pressure cell. *Geotextiles and Geomembranes* 25 (3), 186–193.
- Palmeira, E.M., Gardoni, M.G., 2000. The influence of partial clogging and pressure on the behaviour of geotextiles in drainage systems. *Geosynthetics International* 7 (4–6), 403–431.
- Palmeira, E.M., Gardoni, M.G., 2002. Drainage and filtration properties of nonwoven geotextiles under confinement using different experimental techniques. *Geotextiles and Geomembranes* 20 (2), 97–115.
- Richards, L.A., 1931. Capillary conduction of liquids through porous mediums. *Physics* 1, 318–333.
- Stormont, J.C., Henry, K.S., Evans, T.M., 1997. Water retention functions of four nonwoven polypropylene geotextiles. *Geosynthetics International* 4 (6), 661–672.
- Stormont, J.C., Morris, C.E., 2000. Characterization of unsaturated nonwoven geotextiles, *Advances in Unsaturated Geotechnics*, Shackelford. In: Houston, C.D., Chang, S.L.N.Y. (Eds.), *Geotechnical Special Publication No. 99, Proceedings of sessions of Geo-Denver 2000* sponsored by the Geo-Institute of the ASCE, Reston, Virginia, USA, pp. 529–42.
- SVFlux, 2004. *SoilVision*. Version 5.10. SoilVision Systems Ltd, Saskatoon, Canada.